



# CHORUS

This is the accepted manuscript made available via CHORUS. The article has been published as:

## Magnetic phase diagram of magnetoelectric $\text{LiMnPO}_4$

Rasmus Toft-Petersen, Niels H. Andersen, Haifeng Li, Jiyang Li, Wei Tian, Sergey L. Bud'ko, Thomas B. S. Jensen, Christof Niedermayer, Mark Laver, Oksana Zaharko, Jeffrey W. Lynn, and David Vaknin

Phys. Rev. B **85**, 224415 — Published 14 June 2012

DOI: [10.1103/PhysRevB.85.224415](https://doi.org/10.1103/PhysRevB.85.224415)

# Magnetic phase diagram of magnetoelectric LiMnPO<sub>4</sub>

Rasmus Toft-Petersen,<sup>1,2</sup> Niels H. Andersen,<sup>1</sup> Haifeng Li,<sup>3</sup> Jiying Li,<sup>3</sup> Wei Tian,<sup>3</sup> Sergey L. Bud'ko,<sup>3</sup> Thomas B. S. Jensen,<sup>1</sup> Christof Niedermayer,<sup>4</sup> Mark Laver,<sup>1,4,5</sup> Oksana Zaharko,<sup>4</sup> Jeffrey W. Lynn,<sup>6</sup> and David Vaknin<sup>3</sup>

<sup>1</sup>Department of Physics, Technical University of Denmark, DK-2800 Kgs. Lyngby, Denmark

<sup>2</sup>Helmholtz Zentrum Berlin for Materials and Energy, D-14109 Berlin, Germany

<sup>3</sup>Ames Laboratory and Department of Physics and Astronomy, Iowa State University, Ames, Iowa 50011, USA

<sup>4</sup>Laboratory for Neutron Scattering, Paul Scherrer Institut, CH-5232 Villigen, Switzerland

<sup>5</sup>Niels Bohr Institute, University of Copenhagen, DK-2100 Copenhagen, Denmark

<sup>6</sup>NIST Center for Neutron Research, National Institute of Standards and Technology, Gaithersburg, MD 20899, USA

(Dated: June 4, 2012)

The nature of the spin-flop (SF) transition in the magnetoelectric quasi-2D Heisenberg system LiMnPO<sub>4</sub> is studied in fields applied along the *a* axis. A refinement of the magnetic structure using neutron diffraction data in the SF phase reveals that the spins re-orient from being parallel to the *a* axis to be nearly along the *c* axis at magnetic fields between 4 and 4.7 T, depending on temperature. The low-field antiferromagnetic phase-boundary is shown to join the spin-flop line tangentially at the so-called *bi-critical point*, where there is a suppression of the ordering temperature. At the bi-critical field, we observe an increased intensity of the Lorentz broadened elastic scattering at magnetic Bragg peaks above  $T_N$  as compared to zero field and 10 T, without an increase in peak width. This suggests an increased *density* of fluctuations at the bi-critical field as compared to zero field.

PACS numbers:

## I. INTRODUCTION

Magnetoelectric materials exhibiting a coupling between magnetic and ferroelectric order parameters, such as  $RMnO_3$ <sup>1</sup> (where *R* is a rare earth element) and the charge-ordered  $LuFe_2O_4$ ,<sup>2</sup> have drawn particular interests due to scientific challenges to unravel the coupling mechanism, as well as for their potential applications<sup>3,4</sup>. The *lithium-ortho-phosphates* LiMPO<sub>4</sub> (*M* = Mn, Co, Fe or Ni) - which are also candidates for cathode materials<sup>5</sup> - all exhibit a magnetoelectric (ME) effect in their low-temperature antiferromagnetic (AFM) phases<sup>6</sup>. Contrary to the other lithium ortho-phosphates which have only off-diagonal non-zero ME-tensor elements, all the diagonal elements of the ME tensor of LiMnPO<sub>4</sub> are non-zero.<sup>6</sup> In LiNiPO<sub>4</sub>, orbital contributions (in the form of Dzyaloshinsky-Moriya interactions or anisotropic exchange) and detailed knowledge of the magnetic structure are crucial in order to explain the ME effect.<sup>7</sup> In LiCoPO<sub>4</sub>, such orbital contributions are very strong and can also be significant in order to explain the very large ME effect.<sup>6,8</sup> However, the ground state of the free Mn<sup>2+</sup>-ion has  $S = 5/2$  and  $L = 0$ , and hence the spin-orbit coupling - that also induces the single ion anisotropy term - is practically absent here. In Ref. 9, an investigation of the spin excitations revealed that there are three relatively strong exchange couplings in the *bc*-plane ( $J_{bc} \sim 0.5$  meV) and two much weaker out-of-plane couplings ( $J_a \sim 0.05$  meV) as in the other lithium orthophosphates<sup>10,11</sup>. As expected, a very weak single ion anisotropy ( $D \approx 0.008$  meV) was found, compared to the strongest in-plane nearest-neighbour exchange interactions. Thus, LiMnPO<sub>4</sub> is a pseudo-2D Heisenberg system and has been found to exhibit a spin-flop<sup>12-15</sup>

transition - which is a nearly 90° rotation of antiferromagnetically ordered spins - at  $4 \text{ T} < \mu_0 H_{SF} < 4.7 \text{ T}$  applied along the easy *a* axis.<sup>16,17</sup> The low field magnetic and the spin-flopped structures as determined herein are shown in figure 1.

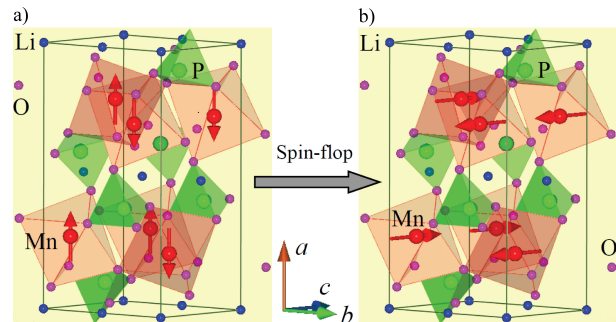


FIG. 1: (Color online) Crystal and magnetic structure of LiMnPO<sub>4</sub>. a) Zero field magnetic structure polarized along the crystallographic *a* axis in the AFM phase at low temperatures. b) The proposed flopped spin structure at  $H > H_{SF}$  applied along *a*.

In SF systems, the so-called *spin-flop bi-critical point* - where the AFM and SF phases join with the paramagnetic phase at  $(T_b, H_b)$  - has been extensively investigated, both theoretically<sup>18-20</sup> and experimentally.<sup>21,22</sup> In 2D *quantum* Heisenberg systems, spin flopping bears an analogy with the Mott-insulator-to-superconductor transition<sup>23</sup> in high temperature superconductors (where the tuning parameter is the chemical potential instead of the magnetic field), which also show a bi-critical point.<sup>24</sup> The bi-critical SF behavior of a more classical 2D-Heisenberg  $S=5/2$  system has also been studied in this context.<sup>25</sup>

In this work, we present bulk magnetization and neutron diffraction studies of the SF transition in  $\text{LiMnPO}_4$ , clarifying the magnetic structure in the SF phase which could be magnetoelectric. We analyze the contribution of the classical dipole-dipole (d-d) to the magnetic anisotropy, and show the necessity of higher order orbital modifications to the otherwise  $L = 0$  ground state. In addition, the magnetic phase diagram has been determined for magnetic fields applied along the easy  $a$  axis, including a thorough investigation of the bi-critical point. The shape of the phase boundaries are shown to be in accordance with the prediction of Fisher in Ref. 20. Finally, the neutron diffraction intensity from the critical scattering above  $T_N$  is shown to be significantly increased near the bi-critical point. This is due to the vanishing *effective* anisotropy at the SF field and suggests a co-existence of fluctuations with two different spin polarizations.

## II. MAGNETIC STRUCTURE AND ANISOTROPY IN $\text{LiMnPO}_4$

$\text{LiMnPO}_4$  has orthorhombic crystal structure with space group  $Pnma$  and lattice parameters  $a = 10.46$  Å,  $b = 6.1$  Å and  $c = 4.75$  Å.<sup>26</sup> It has four magnetic  $\text{Mn}^{2+}$ -ions in each unit cell with spin  $S = 5/2$ , situated at  $\mathbf{r}_1 = (0.278, 0.25, 0.972)$ ,  $\mathbf{r}_2 = (0.778, 0.25, 0.528)$ ,  $\mathbf{r}_3 = (0.722, 0.75, 0.028)$  and  $\mathbf{r}_4 = (0.222, 0.75, 0.472)$ , as shown in Fig. 1. At zero field, the system displays long-range AFM order at temperatures below  $T_N = 33.85$  K,<sup>27,28</sup>. The magnetic structure can be described in terms of the irreducible representations<sup>7,29</sup> of the  $Pnma$  symmetry group. The zero field AFM spin structure determined in Refs. 27 and 28 has the configuration  $(+, +, -, -)$  on the sites  $\mathbf{r}_i$  with increasing  $i = 1, \dots, 4$  and magnetic moments parallel to the crystallographic  $a$  axis - called the  $C_x$ -type structure. Basically, this spin structure has ferromagnetic  $ac$ -planes alternating along  $b$  with the periodicity of the lattice, hence described by the wave vector  $\mathbf{Q}_{\text{AFM}} = (0, 1, 0)$ .

Due to the weak orbital effects ( $L = 0$ ), the magnetic anisotropy of  $\text{LiMnPO}_4$  is very small. This implies that the magnetic anisotropy due to the classical dipole-dipole ( $dd$ ) interaction becomes important. The  $dd$  energy can be written as

$$\mathcal{H}_{dd} = -\frac{1}{2} \sum_{ij} \sum_{\alpha\beta} \mathcal{J}_{\alpha\beta}^{dd}(ij) S_i^\alpha S_j^\beta, \quad (1)$$

where  $i$  and  $j$  denote the magnetic ions in the lattice, and  $\alpha$  and  $\beta$  are the  $a(x)$ ,  $b(y)$ , or  $c(z)$  directions in the crystal.<sup>30</sup> The sum needs to be over all magnetic ions in the lattice. Using an Ewald's summation method,<sup>31</sup> the Fourier components of the diagonal  $dd$  coupling tensor at  $\mathbf{Q}_{\text{AFM}}$  can be calculated to be  $\mathcal{J}_{aa}^{dd}(\mathbf{Q}_{\text{AFM}}) = 0.0088$  meV,  $\mathcal{J}_{bb}^{dd}(\mathbf{Q}_{\text{AFM}}) = -0.0131$  meV and  $\mathcal{J}_{cc}^{dd}(\mathbf{Q}_{\text{AFM}}) = 0.0043$  meV.<sup>32</sup> The  $dd$  interaction contributes to the effective single-ion anisotropy parameters defined in Ref. 9 with contributions which are  $D_c^{dd} = 0.00278$  meV and  $D_b^{dd} =$

$0.01370$  meV. The smallest one, i.e.  $D_c^{dd}$ , is the one determining the SF field  $H_{SF}$  or the spin-wave energy gap at  $\mathbf{Q}_{\text{AFM}}$ ,  $\Delta E = g\mu_B\mu_0 H_{SF}$ . Depending on the estimate of the exchange energy (using either the exchange parameters determined by Li *et al.*<sup>9</sup> or the magnetization measured above  $H_{SF}$  [see Fig. 3(b)]), the value of  $\mu_0 H_{SF} = 4.0$  T, corresponding to  $\Delta E = 0.46$  meV, determines the effective value  $D_c^{eff}$  to lie in the interval between 0.0050 and 0.0069 meV.<sup>32</sup> Hence the  $dd$ -interaction is important but accounts only for about half the anisotropy shown by the system. The remaining part has to be due to higher-order orbital modifications of the ground state. These significant orbital modifications are possibly due to the low crystal field symmetry (in  $\text{LiMnPO}_4$ , the  $\text{Mn}^{2+}$  ions are situated within *distorted* octahedra), and are expected to increase with decreasing local symmetry. The anisotropy terms induced by these modifications are very weak - but of the same order of magnitude as possible anisotropic exchange terms in  $\text{LiNiPO}_4$   $J_{ex}^{ani} \sim (\Delta g/g)^2 J_{ex} \sim 0.01$  meV.<sup>7,11,33</sup> In  $\text{LiCoPO}_4$  however, possible anisotropic exchange terms could be an order of magnitude stronger as  $(\Delta g/g)^2 J_{ex} \sim 0.1$  meV. It should also be noted that the ME effect in  $\text{LiMnPO}_4$  is the weakest of the lithium-orthophosphates (peaking at 1/40 of that in  $\text{LiCoPO}_4$ <sup>6</sup>). Furthermore, these orbital modifications could be the cause of the previously observed zero field weak ferromagnetism in  $\text{LiMnPO}_4$ <sup>34</sup>.

## III. EXPERIMENTAL DETAILS

High-quality  $\text{LiMnPO}_4$  single crystals were grown by standard flux growth technique.<sup>35</sup> The phase purity was confirmed by X-ray powder diffraction. The same single crystal of irregular shape and a weight of 220.14 mg was used in all the experiments presented in this paper.

A CRYOGENIC cryogen free measurement system (CFMS) at the Technical University of Denmark was used to perform vibrating sample magnetization (VSM) measurements. The crystal was oriented on an X-ray Laue camera, glued onto a rigid plastic rod and mounted in the CFMS with the  $a$  axis aligned along the magnetic field within  $0.4^\circ$ . Measurements were performed in magnetic fields between 0 and 12 T applied along the crystallographic  $a$  axis at  $2 K < T < 40 K$ .

To examine the magnetic structure in the SF phase, neutron diffraction experiments were performed using the TriCS diffractometer at the Paul Scherrer Institute (PSI). The crystal was glued to an aluminium sample holder, mounted with the crystallographic  $a$  axis vertical within  $0.4^\circ$  in a 6 T Oxford cryomagnet (the maximum field was 4.5 T at the time of the experiment). The cryomagnet has a large vertical opening that allows TriCS to measure three non-equivalent scattering planes. Vertical and horizontal collimations between the sample and the monochromator were both  $40'$ . The incoming beam propagates in a nose ending in a 10 mm circular aperture.  $80'$  collimation was used between the sample and

the detector. The neutron wavelength used at TriCS was 1.178 Å.

To examine the magnetic phase boundaries, neutron diffraction experiments were performed using the RITA-II triple axis spectrometer at the PSI with an Oxford 15 T cryomagnet. The incoming and outgoing neutron energy was 5 meV. A 40' collimator was inserted between the monochromator and the sample, and a coarse collimation was used between the sample and the analyzer. The crystal was mounted with the  $b$  and  $c$  axis in the scattering plane. The  $a$  axis turned out to be misaligned by about  $2^\circ$  with respect to the vertical field. In the RITA-II experiment, emphasis was on the ordering phase boundaries of the AFM and SF phases. These phase boundaries were measured by performing full omega scans of the (010) peak reflecting both the low field AFM and and the SF main structure components, using the same temperature adjustment scheme at all fields. The measurements were all performed when the temperature had stabilized within  $0.01^\circ$  K.

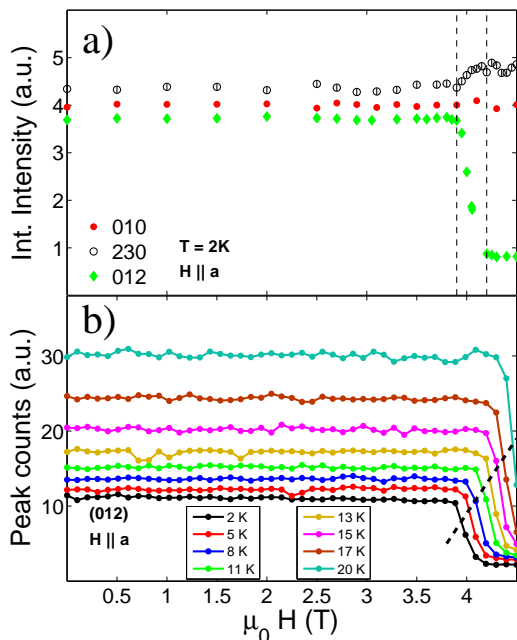


FIG. 2: (Color online) (a) Integrated intensities of the (010), (012) and (230) peaks as a function of field (the intensities of peaks (012) and (230) are scaled by factors 4 and 6 for comparison). Using table I, the data are consistent with a C-type flop of spin polarization from  $a$  to  $c$ . The statistical errors are comparable to or smaller than the markers. (b) Peak intensity of (012) as a function of field at various temperatures (scaled for the sake of illustration) used for phase boundary determination.

## IV. RESULTS AND DISCUSSION

### A. Magnetic structure and spin-flop in $\text{LiMnPO}_4$

The C-type spin-configuration is mainly reflected in reciprocal lattice points with (even, odd, even) or (odd, even, odd) indices. Furthermore, the magnetic neutron scattering intensity is proportional to the square of the so-called *spin polarisation factor* -  $\mathbf{P}_i(\mathbf{Q}) = \hat{\mathbf{Q}} \times (\hat{\mathbf{e}}_i^m \times \hat{\mathbf{Q}})$ , where  $i = x, y, z$  is along the crystallographic  $a, b$  and  $c$  axes respectively,  $\hat{\mathbf{e}}_i^m$  is a unit vector along the spin polarization and  $\hat{\mathbf{Q}}$  is a unit vector directed along the neutron momentum transfer.

	$P_x^2$	$P_y^2$	$P_z^2$	$P_z^2/P_x^2$	$I_{4.5T}^M/I_{0T}^M$
(0, 1, 0)	1	0	1	1	1.01(1)
(0, 1, 2)	1	0.86	0.14	0.14	0.22(1)
(2, 3, 0)	0.87	0.13	1	1.15	1.10(3)

TABLE I: Squared spin polarization factors evaluated for spin polarisation along  $x, y$  and  $z$ , for the three peaks used to establish the flopped structure. The expected and observed intensities in the SF phase are given, normalized to the zero field intensity.

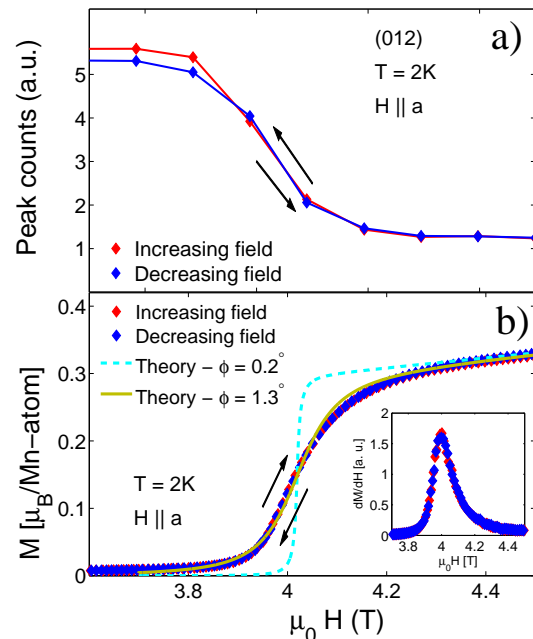


FIG. 3: (Color online) (a) Peak intensity of the (012) peak as a function of applied magnetic field along  $a$  at  $T = 2$  K. No hysteresis is evident. (b) Magnetization versus field at 2 K. The inset shows the differential magnetization. Neither of them show hysteretic behavior. The field induced moment at  $\mu_0 H = 4.5$  T is roughly  $0.325\mu_B$  pr. Mn-atom. The critical field is defined as the maximum slope of the curve in both cases. The two theoretical curves represent the mean field calculations described in the text.

In the TriCS experiment 65 reflections were measured at  $T = 2$  K and  $\mu_0 H = 4.5$  T applied along the  $a$  axis and in zero field at 60 K in the paramagnetic state. Furthermore, a thorough search was made for zero field spin canting components (as observed in  $\text{LiNiPO}_4$ <sup>7</sup>) and zero field co-linear spin rotations (as observed in  $\text{LiCoPO}_4$ <sup>36</sup>) at 2 K, but none were found. A first estimate of the magnetic structure in the SF phase is readily obtained by considering the three key reflections - (010), (012) and (230), listed in table I. As these peaks mainly reflect a C-type structure, but with different spin polarization factors, they will give information about the direction of the magnetic moments in the SF phase, provided that the C-type structure remains after the spin flop. This is expected since the spin structure is determined by the exchange constants. The squared spin polarization factors for these three reflections and the observed change in intensity can be found in table I. The integrated intensity obtained from performing full omega-scans of these reflections as a function of magnetic field is plotted in figure 2 a). As evident, the (010) reflection has constant intensity through the SF phase transition within error (error bars represent one standard deviation). This provides evidence that the SF phase retains the zero field C-type spin-structure throughout the SF transition and the spin polarization is in the  $ac$ -plane. The slight increase of the intensity of the (230) and the drastic decrease in the intensity of the (012) peak (see table I), confirms that the ordered moments are aligned along the  $c$  axis in the SF phase. The decrease of the (012) peak intensity is less than predicted by the spin polarization factors. However, the crystal size and the magnitudes of the ordered moments ( $S = 5/2$ ) make extinction very probable for the strong reflections. The change of magnetic intensity of the (012) reflection is caused by two simultaneous events - moment rearrangement and extinction. Due to the spin-flop the magnetic intensity decreases and is therefore less affected by extinction. We define the critical SF field at the maximum slope of the (012) peak intensity as a function of field. Figure 2 b) shows the field-dependence of the (012) peak intensity at temperatures between 2 and 20 K. It is evident that the critical field increases slightly with temperature up to 20 K.

A more detailed refinement of the magnetic structure at 2 K and 4.5 T was obtained by using the FullProf package<sup>37</sup>. Due to the aforementioned extinction effects, the strongest magnetic reflections were not used in the refinements. The remaining 48 measured magnetic peaks were used to refine the structure within a  $c_1 C_z + c_2 F_x$  configuration space, where  $c_1$  and  $c_2$  are free parameters and  $c_2$  describes the field induced ferromagnetic component,  $F_x$ , along the  $a$ -axis. The result was  $c_1 = 3.93(3)\mu_B$  and  $c_2 = 0.37(6)\mu_B$  with  $\chi^2 = 5.93$ , giving a field induced canting angle of  $5.4(9)^\circ$  from the  $c$  axis toward the  $a$  axis. The relatively high value of  $\chi^2$  is most probably due to systematic errors caused by anisotropic absorption in the magnet. To examine the hysteretic behavior of the SF transition, the peak intensity of the (012) re-

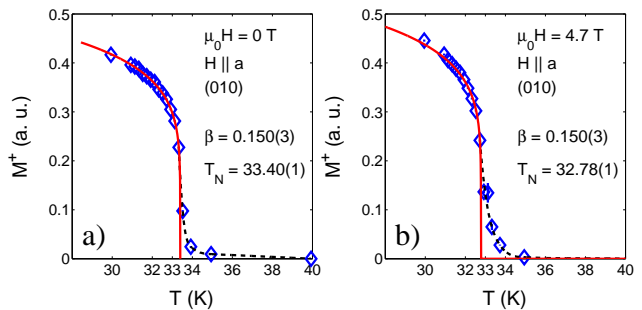


FIG. 4: (Color online) Sub-lattice magnetization (order parameter) measured by neutron diffraction at RITA-II as a function of temperature in zero field (a), and at  $\mu_0 H_b = 4.7$  T (b). The red lines represent power law fits to the staggered magnetization, and the dashed lines are guides to the eye depicting the critical scattering above  $T_N$  which is slightly increased at  $H = H_b$ .

flexion was measured at  $T = 2$  K for increasing and decreasing field, respectively. The result is plotted in Fig. 3 (a) along with the field dependency of the magnetization as obtained from VSM measurements (b) at  $T = 2$  K. Neither the neutron diffraction nor the magnetization data presented in Fig. 3 show signs of hysteresis. It should be noted, however, that an early molecular field analysis of the nature of the spin-flop transition in Ref. 38 predicted that first order behavior can only be expected if the angle between the magnetic field and the easy axis  $\phi < \phi_c = 28.6^\circ H_A/H_{EX}$ , where  $H_A$  and  $H_{EX}$  are the anisotropy and exchange fields, respectively. Using the exchange parameters reported in Ref. 9 and the anisotropies determined in this work,  $\phi_c \approx 0.2^\circ$  for  $\text{LiMnPO}_4$ .<sup>32</sup> The magnetization curve at 2 K has been calculated by means of mean field theory using  $D_c^{eff} = 0.0069$  meV,  $J(\mathbf{Q}_{AFM}) - J(0) = 3.15$  meV for field misalignments of  $\phi = 0.2^\circ$  and  $\phi = 1.3^\circ$ , respectively (see Fig. 3b)<sup>32</sup>. The curve for a  $1.3^\circ$  misalignment describes the magnetization data well.

In conclusion, we have shown that the SF structure is confined to the crystallographic  $ac$ -plane when the field is ramped through the SF transition, and it retains the C-type zero field configuration, but the spins are rotated from the  $a$  axis to the  $c$  axis with a slight field induced ferromagnetic canting along the field. The field induced moment is roughly  $0.325\mu_B$  (as evident in figure 3 b) which suggests a canting angle of  $3.7^\circ$ , which is a little lower than the canting angle obtained from the refinement of the neutron diffraction data. A continuous SF transition is observed by both neutron diffraction and VSM measurements. Mean field calculations account for the magnetization data if the crystal is misaligned by  $1.3$  degrees with respect to the field. Although the alignment on the Laue camera was within  $0.4$  degrees this cannot be assured in the CFMS. Since the SF phase has the same spin-configuration as the AFM phase - and as  $\text{LiNiPO}_4$  exhibits a ME effect in its  $C_z$ -type AFM phase - a magnetoelectric SF phase is indeed possible. A future study of

the ME-tensor components in the SF phase of  $\text{LiMnPO}_4$  could be helpful in determining the microscopic origin of the ME-effect in this material.

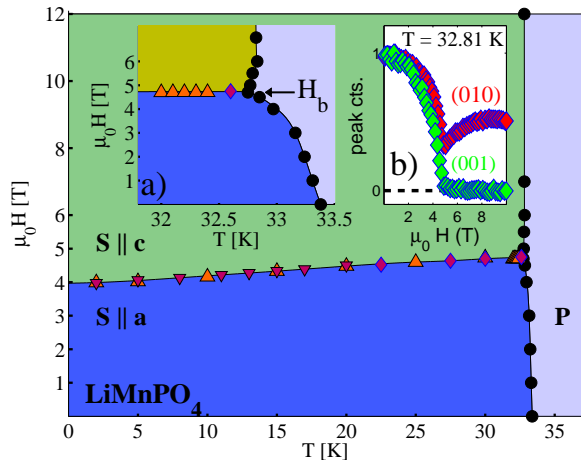


FIG. 5: (Color online) Magnetic phase diagram of  $\text{LiMnPO}_4$  for fields applied along  $a$ . The up-pointing orange triangles represent the critical fields as measured by VSM magnetization measurements. The down-pointing purple triangles are the critical fields as determined by the TriCS measurements of the (012) reflection, and the purple diamonds represent the critical fields as determined by the RITA-II measurement of the (001) reflection as a function of field. The black circles represent the ordering temperature as found from power-law fits to the integrated intensity of the (010) reflection as measured on RITA-II. Inset a) shows the phase boundary close to the bi-critical point. Inset b) shows field scans of the (010) and (001) peak intensities at 32.81 K, which is slightly above  $T_b$ .

## B. Phase diagram and bi-critical fluctuations

The spin-flop phase boundary has been measured using both neutron diffraction (TriCS at low temperatures and RITA-II near  $T_N$ ) and VSM magnetization measurements. The magnetic phase boundary of both the AFM and SF phases has been measured at RITA-II using the (010) peak associated with the  $C_x$  and  $C_z$  spin components. Figure 4 shows the sub-lattice magnetization  $M^\dagger \propto \sqrt{I_{010}}$ , where  $I_{010}$  is the integrated intensity of the (010) peak, as a function of temperature at 0 and 4.7 T. The ordering temperature at any given field was found by fitting the intensities - determined by Gaussian fits to the measured rocking curves with a FWHM fixed to the width of the resolution function - to a power-law  $M^\dagger(T) = A(T_N - T)^\beta$ . The zero field ordering temperature is determined to be  $T_N = 33.40(1)$  K which is a little lower than those determined in Refs. 9,27. The critical exponent is determined to be  $\beta = 0.150(3)$ , which is slightly higher than the previously found value<sup>9</sup> ( $\beta = 0.126(17)$ ). This could be due to the fact that in this work only a reduced temperature range in the vicinity around  $T_N$

is used for fitting. While a genuine 2D-Heisenberg system does not order it is well established that weak inter-plane couplings cause magnetic ordering as observed. The  $\beta = 0.150(3)$  value observed in the present system is in full agreement with the result obtained in the classical pseudo-2D system  $\text{K}_2\text{MnF}_4$  with  $\beta = 0.15(1)$ .<sup>39</sup> Furthermore, there is significantly less critical scattering compared to the results in Ref. 9, where intensity was clearly observed up to  $1.5T_N$ . However, the energy resolution at RITA-II is much better than that in Ref. 9 (0.2 meV in this work compared to 1 meV), which supports the suggestion that the critical scattering is dynamical<sup>9</sup>.

Using the same procedure as in zero field, the critical ordering temperature was determined for fields up to 12 T applied along  $a$ , with focus on the bi-critical point at  $(T_b, H_b)$ . The resulting phase diagram is shown on figure 5. As evident in Fig. 5 the spin-flop phase boundary is sloping with the critical field increasing from 4 T at 2 K to 4.7 T at the bi-critical point. The ordering temperature at the bi-critical field is  $T_b = 32.78$  K, which is slightly lower than at zero field. The inset, Fig. 5a, shows that the AFM phase boundary meets the spin-flop line almost *tangentially*, and the ordering temperatures of both the AFM and SF phases are suppressed at the bi-critical field, as predicted by Fisher in Ref. 20. The suppression of the ordering temperature of the SF phase at  $\mu_0 H = \mu_0 H_b$  is confirmed by the re-entrance of the (010) intensity above 4.7 T (see the field scan in inset b to Fig. 5).

At the bi-critical field, two spin polarization states along the  $a$ - and  $c$  directions have the same energy, and the ordering temperature is suppressed. We explore the bi-critical region by conducting identical L-scans through the magnetic (0 1 0) reflection at various temperatures in the range  $T_N + 0.1 \text{ K} < T < T_N + 4 \text{ K}$ , at zero field, at the bi-critical field and at  $\mu_0 H = 10$  T. This way the exact same volume of  $(\mathbf{Q}, \omega)$ -space is probed at comparable temperature intervals for the three fields. Figure 6 shows four of these L-scans at zero field and at  $\mu_0 H_b = 4.7$  T. A significant increase in peak intensity at the bi-critical field is evident. We examined whether this increase in amplitude is accompanied by an increase of the correlation length, which proved not to be the case. It should be recalled that with an energy resolution of only 0.2 meV on RITA-II, we measure in the near-elastic regime. However, an increase in the correlation lengths at the bi-critical field should still be clearly seen even in this narrow energy interval. The peaks were fit to a Lorentzian -  $S \sim 1/(q^2 + \kappa^2)$  - that is convoluted with a fixed instrumental Gaussian resolution function. A measure of the correlation lengths along  $c$  -  $\xi_c(T)$  - was found using  $\xi = c/2\pi\kappa$ , where  $\kappa$  (in r.l.u) is the half width half maximum of the Lorentzian part of the fit. The results are shown in Fig. 7a along with the integrated intensities obtained from the fits (Fig. 7b).

The correlation lengths have been fitted to a simple power law -  $\xi(T) = A/t(H)^\nu$  - where  $t(H) = \frac{T - T_N(H)}{T_N(H)}$  is the reduced temperature. The fits are reasonable and similar for all fields, with an average exponent of  $\nu =$

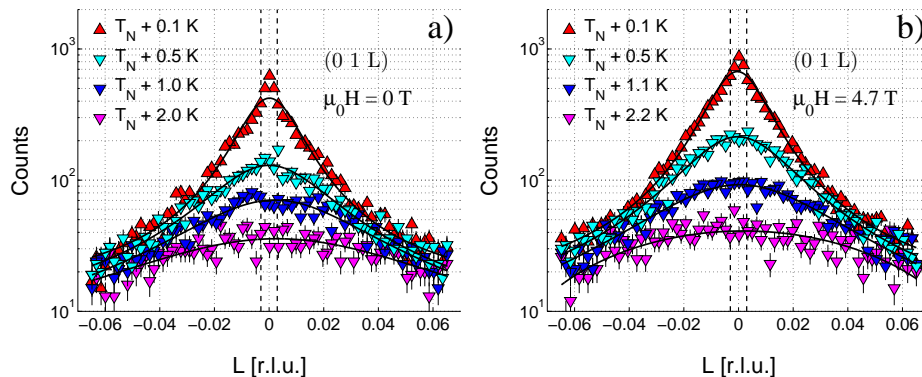


FIG. 6: (Color online) a) L-scans of the (010) peak at four selected temperatures above  $T_N$  at  $\mu_0 H = 0$  T plotted on a logarithmic scale; the Lorentzian shape is clearly evident. b) L-scans of the (010) peak at similar temperatures relative to  $T_b$  at  $\mu_0 H = H_b = 4.7$  T. The peak shapes are similar to those obtained at zero field, but with a significantly increased amplitude. The dashed lines indicates the FWHM of the (010) Bragg peak which is 0.006 r. l. u.

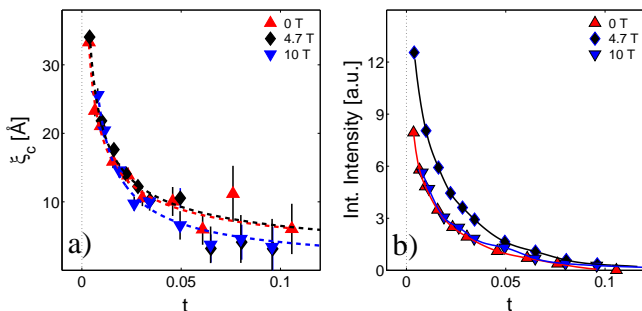


FIG. 7: (Color online) a) The correlation lengths as a function of temperature relative to  $T_N(H)$  as obtained from Voigt fits to peaks such as those depicted in figure 6 for 0, 4.7 and 10 T applied along  $a$ . The correlation lengths exhibit similar magnitude and dependency on temperature for all fields. The dashed lines mark the fits as described in the text. b) The integrated intensity as a function of relative temperature for 0, 4.7 and 10 T applied along  $a$ . A significant increase in intensity is evident at the bi-critical field  $\mu_0 H_b = 4.7$  T. The solid lines are guides to the eye.

0.57(6). As evident in figure 7a, the three data sets are practically overlapping and there is no significant increase in correlation length at the bi-critical field along the crystallographic  $c$  axis. Due to the vertical focusing of the spectrometer a large part of the Brillouin-zone along the vertically oriented  $a$  axis is effectively measured. Assuming that there is no change in the correlation length at the bi-critical field along the  $b$  axis, this suggests that the temperature-dependence of the correlation lengths remains unchanged at all fields. Figure 7b shows the integrated intensity as a function of  $t$  at the three fields. The overall increase of intensity at the bi-critical field, as compared with the intensity at 0 and 10 T, is significant. We argue that this increase can only be due to an increased spectral weight  $S(\mathbf{Q}, \omega)$  in the measured volume of  $(\mathbf{Q}, \omega)$ -space at the bi-critical field. A qualitative interpretation of this increase in critical scattering in-

tensity is that either the *density* or the *lifetime* of the critical fluctuations is increased at the bi-critical field. We have no empirical evidence ruling out an increase in the lifetime of the fluctuations. However, due to the field induced isotropy in the  $ac$ -plane, the most intuitive suggestion is that there is a co-existence of fluctuations in two different spin polarization states -  $M_{C_x}^\dagger$  and  $M_{C_z}^\dagger$  - resulting in an overall increase of the density of critical fluctuations.

## V. CONCLUSIONS

In conclusion, the classical d-d interaction has been shown not to be sufficient to explain the weak anisotropy in  $\text{LiMnPO}_4$  as obtained from the SF critical field and the spin gap reported in ref. 9, higher-order orbital modifications to the ground state are necessary. The spin flop in  $\text{LiMnPO}_4$  has been determined to occur solely as a reorientation within the  $ac$  plane. The SF structure is a C-type configuration polarized along the  $c$  axis, consistent with the fact that the  $b$  axis is the hard axis of the d-d interaction. The bi-critical phase boundaries have been examined and found to be in accordance with theoretical predictions<sup>20</sup>. The AFM phase boundary meets the spin flop line almost tangentially and there is a suppression of the ordering temperatures of both the AFM and SF phase at the bi-critical field. Furthermore, the critical fluctuations have been examined at three fields. While there is no significant change in the temperature-dependence of the Lorentzian peak widths, we find that the *intensity* of the critical scattering is significantly increased at the bi-critical field - both when compared to zero field and to 10 T applied along  $a$ . This suggests the co-existence of critical fluctuations of the two different phases with average moment direction along the crystallographic  $a$ - and  $c$ -direction, respectively, possibly both magnetoelectric in nature. This increases the overall density of fluctuations near the bi-critical point, as observed.

### Acknowledgments

Jens Jensen of the University of Copenhagen is greatly acknowledged for illuminating discussions, for determining the anisotropy and for performing the mean field calculations of the magnetization. The authors would like to thank Ellen Fogh, Dennis Lund Lorenzen, Nelson Walther Bayas and Mikkel Rønne Lotz, for useful assistance during the RITA-II experiment. Work was supported by the Danish Agency for Science, Technology and Innovation under DANSCATT and by the Swiss NSF via contract PP002-102831. The manuscript has been authored, in whole or in part, under Contract No. DE-AC02-07CH11358 with the U.S. Department of Energy. Neutron experiments were performed at the SINQ neutron spallation source at the Paul Scherrer Institute, Switzerland.



- 
- <sup>1</sup> T. Kimura, T. Goto, H. Shintani, K. Ishizaka, T. Arima, and Y. Tokura, *Nature* **426**, 55 (2003).
- <sup>2</sup> N. Ikeda, et al., *Nature* **436**, 1136 (2005).
- <sup>3</sup> W. Eerenstein, N. D. Mathur and J. F. Scott, *Nature* **442**, 759-765 (2006).
- <sup>4</sup> S. W. Cheong and M. Mostovoy, *Nature Materials* **6**, 13 (2007).
- <sup>5</sup> C. M. Julien, A. Ait-Salah, A. Mauger, and F. Gendron, *Ionics* **12**, 21 (2006)
- <sup>6</sup> M. Mercier, Ph.D. thesis, Université de Grenoble (1969).
- <sup>7</sup> T. B. S. Jensen, N. B. Christensen, M. Kenzelmann, H. M. Rønnow, C. Niedermayer, N. H. Andersen, K. Lefmann, J. Schefer, M. v. Zimmermann, J. Li, J. L. Zarestky, and D. Vaknin, *Phys. Rev. B* **79**, 092412 (2009).
- <sup>8</sup> Rasmus Toft-Petersen, Ph.D. thesis, DTU, Technical University of Denmark (2012).
- <sup>9</sup> Jiyang Li, Wei Tian, Ying Chen, Jerel L. Zarestky, Jeffrey W. Lynn and David Vaknin, *Phys. Rev. B*, **79**, 144410, (2009)
- <sup>10</sup> Wei Tian, Jiyang Li, Jeffrey W. Lynn, Jerel L. Zarestky and David Vaknin, *Phys. Rev. B*, **78**, 184429, (2008)
- <sup>11</sup> T. B. S. Jensen, N. B. Christensen, M. Kenzelmann, H. M. Rønnow, C. Niedermayer, N. H. Andersen, K. Lefmann, M. Jiménez-Ruiz, F. Demmel, J. Li, J. L. Zarestky, and D. Vaknin, *Phys. Rev. B* **79**, 092413 (2009).
- <sup>12</sup> L. Neel, *Ann. Phys. (Paris)* **5**, 232 (1936).
- <sup>13</sup> N. J. Poulis, J. van den Handel, J. Ubbink, J. A. Poulis, and C. J. Gorter, *Phys. Rev.* **82**, 552 (1951).
- <sup>14</sup> D. Lebeugle, D. Colson, A. Forget, M. Viret, A. M. Bataille, and A. Guskasov, *Phys. Rev. Lett.* **100**, 227602 (2008).
- <sup>15</sup> A. N. Bogdanov, A. V. Zhuravlev, and U. K. Roessler, *Phys. Rev. B* **75**, 094425 (2007).
- <sup>16</sup> J. H. Ranicar and P. R. Elliston, *Physics Letters.* **25A**, 720, (1967)
- <sup>17</sup> Wei Tian, Jiyang Li, Haifeng Li, Jeffrey W. Lynn, Jerel L. Zarestky and David Vaknin, *J. Phys. Conference Series*, **251** 012005 (2010)
- <sup>18</sup> David R. Nelson and J. M. Kosterlitz and Michael E. Fisher, *Phys. Rev. Lett.*, **73** 813 (1974)
- <sup>19</sup> Michael E. Fisher and David R. Nelson, *Phys. Rev. Lett.*, **32** 1350 (1974)
- <sup>20</sup> Michael E. Fisher, *Phys. Rev. Lett.*, **34** 1634 (1975)
- <sup>21</sup> H. Rohrer, *Phys. Rev. Lett.*, **34** 1638 (1975)
- <sup>22</sup> J. A. J. Basten and E. Frikke and W. J. M. de Jonge, *Phys. Rev. B*, **22** 1429 (1980)
- <sup>23</sup> E. Demler, W. Hanke and S. Zhang, *Rev. of Mod. Phys.* **76** 909 (2004)
- <sup>24</sup> Xiao Hu, *PRL* **87** 057004-1 (2001)
- <sup>25</sup> R. L. Leheny, R. J. Christianson, R. J. Birgeneau and R. W. Erwin, *PRL* **82** 418-421 (1999)
- <sup>26</sup> S. Geller and J. L. Durand, *Acta Cryst.* **13** 325, (1960)
- <sup>27</sup> J. M. Mays, *Phys. Rev.* **131**, 38 (1963).
- <sup>28</sup> R. E. Newnham and R. P. Santoro and M. J. Redman, *J. Phys. Chem. Solids.*, **26** 445, (1964)
- <sup>29</sup> Rossat-Mignod, *J. Methods of experimental physics* (Academic Press Inc, 1987) Vol. 23, part C, chapter 19.
- <sup>30</sup> J. Jensen and A. R. Mackintosh, *Rare Earth Magnetism: Structures and Excitations* (Clarendon Press, Oxford, 1991); <http://www.nbi.ku.dk/page40667.htm>
- <sup>31</sup> G. J. Bowden and R. G. Clark, *J. Phys. C* **14**, L827 (1981).
- <sup>32</sup> Jens Jensen, private communication.
- <sup>33</sup> Toru Moriya, *Phys. Rev.* **120**, 9198 (1960)
- <sup>34</sup> D. Arcon, et. al., *J. Of Phys. and Chem. Of Solids* **65** 1773 (2004)
- <sup>35</sup> V. I. Fomin, V. P. Genezdilov, V. S. Kurnosov, A. V. Peschanskii, A. V. Yermenko, H. Schmid, J.-P. Rivera, and S. Gentil, *Low Temp. Phys.*, **28**, 203 (2002).
- <sup>36</sup> D. Vaknin and J. L. Zarestky and L. L. Miller and J.-P. Rivera and H. Schmid, *PRB* **65** 224414 (2002)
- <sup>37</sup> J. Rodriguez-Carvajal, *Physica B* **192**, 55-69 (1993)
- <sup>38</sup> H. Rohrer and H. Thomas, *J. Appl. Phys.* **40**, 1025 (1969)
- <sup>39</sup> R.J. Birgenau, H.J. Guggenheim and G. Shirane, *Phys. Rev. B* **8**, 304 (1973)